Biosensors and Bioelectronics 150 (2020) 111928

Contents lists available at ScienceDirect

Biosensors and Bioelectronics

journal homepage: http://www.elsevier.com/locate/bios

A high sensitivity background eliminated fluorescence sensing platform for hyaluronidase activity detection based on Si QDs/HA-δ-FeOOH nanoassembly

Xiang Li [a,**], Tian Wu [a], Yuanqi Fu [a], Xuelian Ding [a], Zhongjian Li [b,c], Guifen Zhu [a], Jing Fan [a,*]

[a] School of Environment, Henan Key Laboratory for Environmental Pollution Control, Key Laboratory for Yellow River and Huai River Water Environment and Pollution Control, Ministry of Education, Henan Normal University, Xinxiang, Henan, 453007, PR China
[b] Xingyang People's Hospital, Xingyang, Henan, 450100, PR China
[c] Henan Cancer Hospital, Zhengzhou, Henan, 450008, PR China

ARTICLE INFO

Keywords:
Si QDs/HA-δ-FeOOH nanoprobes
Eliminated background signal
Hyaluronidase
High sensitivity

ABSTRACT

Using fluorescent sensors for highly sensitive and selective detection of biomolecules is a very important strategy in clinical diagnoses as well as biomedical applications. But fluorescent sensors usually suffer from high background signal, which greatly hinders their detection sensitivity. In this work, a novel background-eliminated fluorescence assay for sensitive and selective detection of biomolecule has been developed by coupling feroxyhyte nanosheets (δ-FeOOH) with amino-functionalized silicon quantum dot (Si QDs). We select hyaluronidase (HAase) as the modal target to verify the concept. Si QDs/HA-δ-FeOOH nanoassembly was fabricated by self-assembly of positive Si QDs together with negative HA-δ-FeOOH through electrostatic adsorption. By the introduction of hyaluronidase, the nanoassembly exhibits obviously fluorescence signal recovered. Research suggests that under optimized conditions, this strategy exhibits a good linear response to the concentration of HAase in the range of 0.1 to 12 ng/mL. The detection limit for HAase was 0.02 ng/mL (based on 3σ/S), which was three-order lower than most of the reported fluorescence biosensors for the detection of HAase. Furthermore, this new biosensor has already been applied in the study of urine samples, and the detection results were consistent with those obtained by the clinical tests.

1. Introduction

Sensitive and selective detection of biomolecules is very important in the field of early clinical diagnoses, biomedical and environmental applications (Wu and Qu, 2015; Xu et al., 2014). Different strategies have been developed for the biomolecules detection, such as electrochemistry (Chinen et al., 2015), optical methods (Wang et al., 2013) and surface-enhanced Raman scattering (Sinh et al., 2018). Among these strategies, fluorescence methods are particularly interesting due to their high stability, sensitivity, and feasibility of quantification. However, many fluorescence sensors suffer from false-positive signals and high background signals, which decrease their sensitivity in the detection process. To enhance the detection sensitivity of fluorescence sensors, many sensor systems used nanomaterials as "super-quencher" to reduce the background signal (Anichini et al., 2018; Baptista et al., 2015; Zhu et al., 2017). In those sensors, the quenching efficiency reach to 90% is generally considered to be ideal "quenching-off" states. However, the residual fluorescence signals still have an impact on the detection of trace amounts target. Therefore, the development of background elimination fluorescent sensors is particularly important for improving trace analytical performances.

In recent years, a designed method that using magnetic separate properties of magnetic nanoparticles to construct biosensor has attracted great interest (Lin et al., 2017; Yang et al., 2012; Yin et al., 2016). For example, a series of low background signals biosensors have been developed for biomolecules detection by using modified Fe_3O_4 nanoparticles to separate the signals from the sensor solution (Hu et al., 2017; Wang et al., 2017; Zhang et al., 2016). However, most of these sensors need to be modified on the surface of Fe_3O_4, which increases the processing steps and analytical costs. Feroxyhyte (δ-FeOOH) ultrathin

* Corresponding author. School of Environment, Henan Normal University, Xinxiang, Henan, 453007, PR China.
** Corresponding author. School of Environment, Henan Normal University, Xinxiang, Henan, 453007, PR China.
E-mail addresses: xli2011@163.com (X. Li), fanjing@htu.cn (J. Fan).

https://doi.org/10.1016/j.bios.2019.111928
Received 5 July 2019; Received in revised form 25 October 2019; Accepted 25 November 2019
Available online 3 December 2019

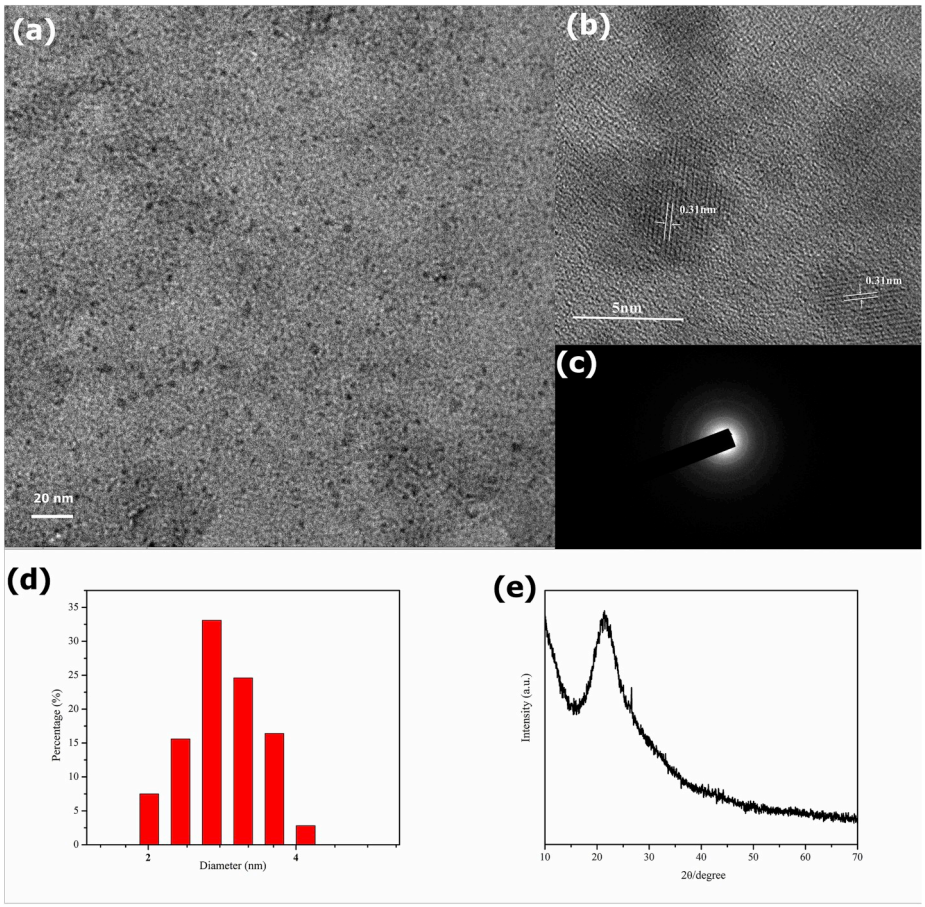

Fig. 1. Characterization of the as-prepared Si QDs. (a), TEM images of the prepared nanomaterials; (b), high-resolution TEM image of the typical Si QDs; (c) the corresponding SAED pattern of Si QDs with the electron beam perpendicular to its basal plane; (d), DLS of the Si QDs; (e) XRD spectrum of the as prepared Si QDs.

nanosheet is a metastable phase in ferrous metal series oxides (Okamoto, 1968). It is a new type of inorganic graphene analogue with ferromagnetic and semiconducting properties. Due to the exotic electronic properties, δ-FeOOHs have been widely used in the field of catalysis (Fan et al., 2016; Lima et al., 2015; Liu et al., 2018a) and adsorption (Faria et al., 2014; Maia et al., 2019). Because of a more significant number of hydroxyls on the δ-FeOOH surface than that of magnetite and maghemite, δ-FeOOH shows excellent water solubility, good biocompatibility and large specific surface area, which provides conditions for the application of ferric hydroxide in the biological system. More importantly, δ-FeOOH possesses the strong magnetic properties at the room temperature, and it is higher than that of various traditional two-dimensional ferromagnetic materials (Chen et al., 2014). Thus, the application of δ-FeOOH nanosheets to construct sensor strategy is worthy of investigation. However, using the magnetic properties of δ-FeOOH to construct the biosensor has not been reported at present.

Hyaluronidase (HAase) is a kind of glycosidase generally exists in nature, and it has been reported that the elevated expression of HAase plays a significant role in many malignant tumors (such as bladder cancer and prostate cancer), and could act as a potential tumor marker (Lokeshwar et al., 2006; Roberts et al., 2014). Thus, seeking for accurate detection methods for the trace amounts of HAase detection have raised to a tough challenge. Recently, some blue emission quantum dots were used for HAase detection based on the electrostatic adsorption (Gu et al., 2016; Ge et al., 2018; Liu et al., 2018b). Although these approaches have their distinct advantages; there still remain some problems to overcome such as high background signal and poor sensitivity. Additionally, it was said that some carbohydrates in cells can emit blue emission (auto fluorescence) under the ultraviolet excitation and biological tissues exhibit higher absorption in blue light region rather than in longer-wavelength regions (Wang et al., 2014b; Liu et al., 2015a; Niu et al., 2015). When using the blue fluorescence emission probes, the signals from the probe molecules would be masked by cellular auto fluorescence, and this will make it difficult to distinguish the probe molecule from the background. Therefore, making the achievement of very low or eliminated background signals is still challenging.

In this work, we put forward a novel background eliminated fluorescence assay strategy for the detection of HAase activity by adopting amino-functionalized green fluorescent Si QDs dots as signal reporters and δ-FeOOH as fluorescence quencher. Compared with the traditional homogeneous fluorescence sensor, this strategy offers several unsurpassed advantages. First, using green fluorescence Si QDs in the complex biological system could avoid the interference of cellular auto fluorescence. Second, using δ-FeOOH as a fluorescence quencher can greatly reduce background signal even to eliminated background signal, thus the sensitivity of the HAase detection is enhanced more than 1000 times as compared with previous fluorescence approaches. Additionally, the δ-FeOOH nanosheets are adopted, for the first time, in the detection of biomolecules, which open up the scope of δ-FeOOH nanosheets in biosensor and biomedical studies.

2. Materials and methods

2.1. Reagents and materials

The green fluorescence Si QDs (Wang et al., 2014a) and two-dimensional δ-FeOOH nanosheets (Chen et al., 2014) were prepared according to the literatures, respectively. Hyaluronic acid sodium salt

(Mw = 1100 KDa) and HAase (608 U/mg) were obtained from Solarbo Technology Co. Ltd. (Beijing, China). Phosphate buffered saline (PBS, 10 mM, pH 6.2) was used in the experiment. All solutions were prepared with distilled water. All chemicals were analytical grade and used without additional purification.

2.2. Apparatus

Images of transmission electron microscopy (TEM) were recorded on a JEM-2100 transmission electron microscope (JEOL, Tokyo, Japan). X-ray diffraction (XRD) pattern was characterized on a X' Pert3 Powder X-ray diffractometer (PANalytical B.V. Almelo, Netherlands). X-ray photoelectron spectrometry (XPS) spectra were gathered on an ESCA-LAB250Xi X-ray photoelectron spectrometer (Thermo Fisher Scientific, Massachusetts, U. S. A). Fourier transform infrared (FT-IR) spectra were recorded on a Spectrum 400F spectrometer (PerkinElmer, Massachusetts, U.S.A). UV–vis spectra were recorded on an UV-T6 spectrophotometer (Purkinie, Beijing, China). Fluorescence spectra were measured on a Cary Eclipse fluorescence spectrometer (Varian, California, U. S. A). The dynamic light scattering (DLS) and zeta potentials were recorded on Zetasizer Nano ZS90 nanoparticle size and zeta potential analyzers (Malvern Instruments, Malvern, U. K.).

2.3. Fabrication of HA-δ-FeOOH

100 μL HA (100 mM) was dispersed in 900 μL PBS buffer containing 1 mg δ-FeOOH, and then the mixed solution was incubated at 37 °C for 30 min. Then, the HA-δ-FeOOH was readily collected using magnetic decantation. The nanoassembly sediments were resuspended in the PBS buffer solution for further use.

2.4. Assay procedures for the detection of HAase activity

For the detection of HAase activity, in the 400 μL of PBS buffer, 20 μL of Si QDs (0.5 mg/mL) was first mixed with 30 μL of HA-δ-FeOOH to form Si QDs/HA-δ-FeOOH nanoprobes. Then different amounts of HAase were added to the nanoprobes solution and incubated for 60 min at 37 °C. The fluorescence spectra of the reaction solutions were measured after magnetic separation. The fluorescence intensity was measured at 520 nm.

2.5. Preparation of the biological samples

For the determination of HAase in real samples, the urine samples included three advanced bladder cancer male patients, three early bladder cancer male patients and three healthy males (obtained from Henan Cancer Hospital) were prepared. This study was approved by the Henan Cancer Hospital Ethics Committee, and all participants provided written informed consent prior to sample collection. Briefly, the urine samples were collected and centrifuged at 3200×*g* at 4 °C for 20 min, and the upper supernatant solution was preserved to serve for further detection. The upper supernatant solutions were diluted 40-fold with PBS, and then they would be used for HAase detection immediately. It is the same situation in the process of HAase detection in real urine samples and the buffer solution.

3. Results and discussion

3.1. Characterization of as-prepared materials

The microstructure and particle size distributions of as-prepared Si QDs were featured by TEM and DLS. TEM images of the dispersed Si QDs in solution were shown in Fig. 1a, it could be seen that the as-prepared Si QDs were spherical and uniform particles and exhibited excellent monodispersity. The HRTEM image (Fig. 1b) and the stripes of concentric circles (Fig. 1c) indicated that the prepared Si QDs possessed good crystallinity. The spacing of 0.31 nm agrees with the (111) lattice spacing, which was in accordance with the literature and demonstrated the formation of Si QDs (Wang et al., 2014). For the size distribution analysis, the diameter of Si QDs existed in the range of 3.1 ± 1.3 nm determined by DLS (Fig. 1d), which showed a satisfactory agreement with TEM. To investigate the chemical state and composition of the Si QDs, the XPS measurements were performed. As seen in Fig. S1, the XPS spectrum clearly showed that Si QDs were comprised of Si, C, N, and O elements. The five peaks at 102.3, 152.68, 285.05, 399.25, and 532.05 eV, which were corresponded to Si 2p, Si 1s, C 1s, N 1s, and O 1s. FT-IR spectrum was also adopted to investigate the surface chemical composition of the as-prepared Si QDs (Fig. S2). As shown in the FT-IR

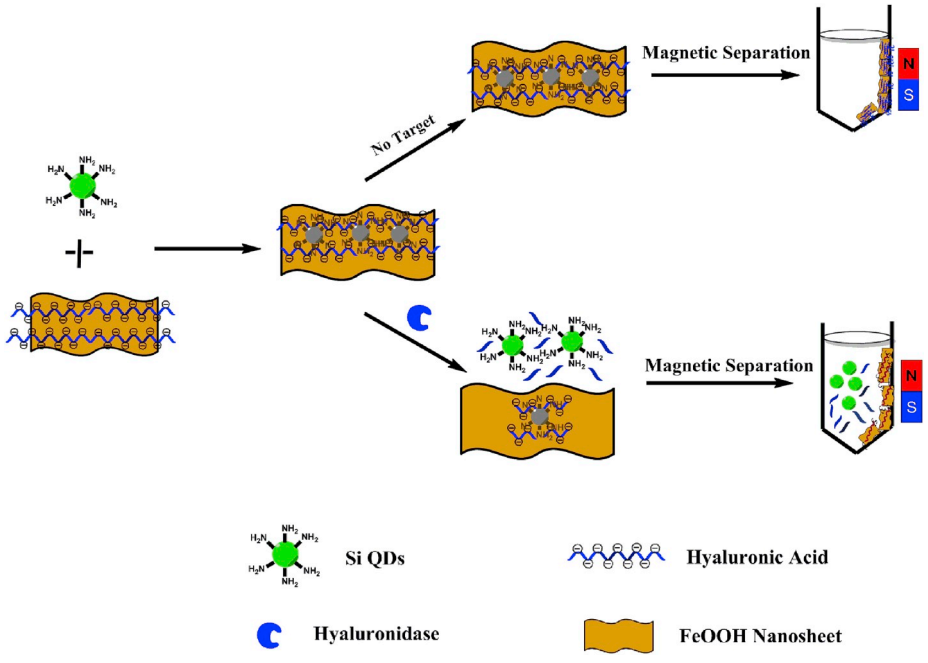

Scheme 1. The schematic representation of the detection of HAase.

spectroscopy, the peak at 3276 cm^{-1} was attributed to N–H bending and the peak at 1643 cm^{-1} indicated the N–H bond bending vibration, all these peaks indicate that the Si–NH_2 moiety on the surface of Si QDs. Additionally, The peak of O–H bending was located at 2926 cm^{-1}, and Si–O–Si was confirmed by the peaks located at 1077 cm^{-1}. Moreover, the X-ray diffraction pattern indicated that Si QDs were in the amorphous phase (Fig. 1e). The fluorescence spectrum of Si QDs was also measured. As given in Fig. S3, the emission wavelength of Si QDs causes red-shift from 460 to 540 nm when the excitation wavelength gradually changed from 340 to 440 nm, which indicated that the as-obtained Si QDs exhibited typical excitation-dependent fluorescence behavior (Song et al., 2016; Li et al., 2018). The Si QDs exhibited high fluorescence emission intensity at 520 nm with green fluorescence upon 420 nm excitation (Fig. S4). Using fluorescein as a reference (QY = 95%, in 0.1 M NaOH) (Brannon and Magde, 1978), the QY of Si QDs in water with the excitation wavelength at 420 nm was found to be 18.2%. Furthermore, the water stability and photostability of Si QDs were also investigated. As shown in Fig. S5, when the pH values changing from 3.0 to 11.0, the fluorescence of the Si QDs was still stable, which indicates that Si QDs had relatively stable fluorescent activity for the pH changes. It can be seen in Fig. S6, the fluorescence of Si QDs was still stable even in the 100 mM NaCl buffer solution, which shows the excellent stability of Si QDs toward high salt conditions. Additionally, Si QDs still exhibits excellent photostability, even after continuous irradiation by using a UV lamp over a period of 120 min (Fig. S7). All these results show that the prepared Si QDs was stable enough for using in biosensing applications.

The as-prepared δ-FeOOH nanosheets were also characterized by TEM. As shown in Fig. S8, the δ-FeOOH nanosheets demonstrate wrinkle and nearly transparent nanosheets, which was similar to the structure of graphene. This result also confirms the ultrathin nanosheet morphology of the as-synthesized δ-FeOOH nanosheets (Chen et al., 2014). More importantly, the δ-FeOOH nanosheets exhibit the high planar surface, which makes it possible for an increased number of Si QDs to be adsorbed on the surfaces of δ-FeOOH nanosheets. The crystalline structures of the prepared δ-FeOOH nanosheets are investigated by XRD. As presented in Fig. S9, the XRD profiles show similar diffraction patterns with δ-FeOOH (JCPDS 77-0247). The prepared δ-FeOOH was yellowish-brown and with a wide light absorption range from the UV to visible region (Fig. S10). So δ-FeOOH could be used as an ideal energy acceptor for diverse chromophores. The magnetic field dependence of magnetization (M–H) curves for the δ-FeOOH ultrathin nanosheets was also measured. As showed in Fig. S11, the magnetic saturation of δ-FeOOH was about 7.2 emu g^{-1}, which was consistent with the reported literature. These results prove that the magnetic δ-FeOOH ultrathin nanosheets have been successfully prepared.

3.2. Principle of sensing HAase

Scheme 1 displayed our detection strategy. HA, as a negatively charged linear mucopolysaccharide, was preferentially interacted with positive δ-FeOOH to form the HA-δ-FeOOHs by electrostatic attraction. Then the Si QDs/HA-δ-FeOOH nanoprobes were fabricated by self-assembly of positive Si QDs and negative HA-δ-FeOOH via electrostatic adsorption (Liu et al., 2015b; Ge et al., 2018). The fluorescence of Si QDs was quenched by HA-δ-FeOOH. In the absence of HAase, the Si QDs could be not released from the surface of δ-FeOOH due to electrostatic self-assembly. After adding an external magnetic field, the Si QDs/HA-δ-FeOOH nanoprobes were adsorbed on the sidewall (non--optical channel) of the cuvette (Fig. S12), the residual fluorescence signals from no complete quenched fluorescence can be readily and thoroughly cleared away, which eliminate the background signal in the solution. However, in the presence of HAase, HA was digested into fragments, which led to the dismantlement of the nano-assembly and the Si QDs were released from the surface of δ-FeOOH, resulting in the recovery of quenched fluorescence. To confirm the feasibility of preparing Si QDs/HA-δ-FeOOH nanoprobe for HAase detection, the zeta potentials

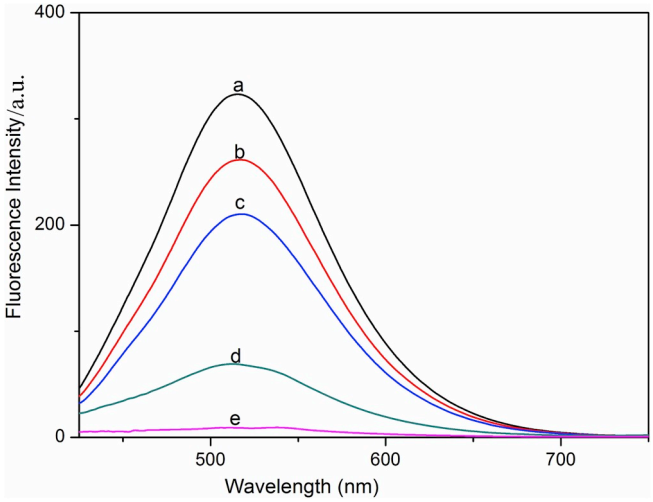

Fig. 2. Fluorescence emission spectra of different sensing systems: (a) Si QDs only; (b) Si QDs + δ-FeOOH; (c) Si QDs + HA-δ-FeOOH + HAase; (d) Si QDs + HA-δ-FeOOH; (e) Si QDs + HA-δ-FeOOH + magnetic separation. Measurements were performed in PBS (10 mM, pH 6.2). [Si QDs] = 0.02 mg/mL, [δ-FeOOH] = 17 μg/mL, [HA-δ-FeOOH] = 17 μg/mL, [HAase] = 10 ng/mL.

of the as-prepared Si QDs, δ-FeOOH, HA-δ-FeOOH and Si QDs/HA-δ-FeOOH nanoassembly were measured in aqueous solution. As shown in Fig. S13, the zeta potentials of Si QDs and δ-FeOOH were about +5.8 and +8.5 mV, respectively. The zeta potential of HA-δ-FeOOH was −34.1 mV, which was mainly due to the negative charge of HA attaching the surface of δ-FeOOH. However, the zeta potential of Si QDs/HA-δ-FeOOH nanoassembly was −7.8 mV, which indicated that the positively charged Si NPs could be electrostatically adsorbed on negatively charged HA-δ-FeOOH, leading to the change of zeta potential of HA-δ-FeOOH from −34.1 to −7.8 mV. Moreover, the variation in the zeta potential of Si QDs/HA-δ-FeOOH nano-assembly was further measured in the presence of HAase. As shown in the Fig. S14, the zeta potential of Si QDs/HA-δ-FeOOH changed from negative charge to positive charge with the progress of enzyme hydrolysis reaction. The zeta potential result confirmed that the long-chain HA was broken down to fragment after HAase digestion, which led to the dismantlement of the nano-assembly as a result of impaired electrostatic interaction, and the Si QDs were released from surface of nano-assembly. Additionally, after using magnetic separation, all δ-FeOOH-containing compounds (such as unreacted Si QDs/HA-δ-FeOOH and δ-FeOOH) were separated from the solution and adsorbed on the sidewall, which was greatly reduced the interaction between the Si QDs with all δ-FeOOH-containing compounds. So the released Si QDs could be left in the solution and the fluorescence intensity was recovered.

Transmission electron microscopy (TEM) was also performed to confirm the formation of the nanoassembly between Si QDs and HA-δ-FeOOH nanosheets. As shown in Fig. S15, the Si QDs were dispersed on the surface of HA-δ-FeOOH nanosheets. The size of Si QDs/HA-δ-FeOOH nanoprobes shows an average of 100 nm by TEM. Then, the effect of pH and ionic strength on the Si QDs/HA-δ-FeOOH nanoprobes was studied. As shown in Figs. S16 and S17, the pH value changing (from 4.0 to 10.0) and ionic strength could not affect the fluorescence intensity of the nanoprobes. All those data show that the nanoprobe is rather stable against pH and ionic strength change, which shows the functions well under physiological conditions.

In order to verify the feasibility of this strategy for HAase detection, the fluorescence spectra of nanoprobe under different conditions were performed. It can be seen in Fig. 2, under 420 nm excitation, Si QDs exhibit strong fluorescence emission at 520 nm (curve a). In the presence of δ-FeOOH, it can be seen that 25% fluorescence of Si QDs was

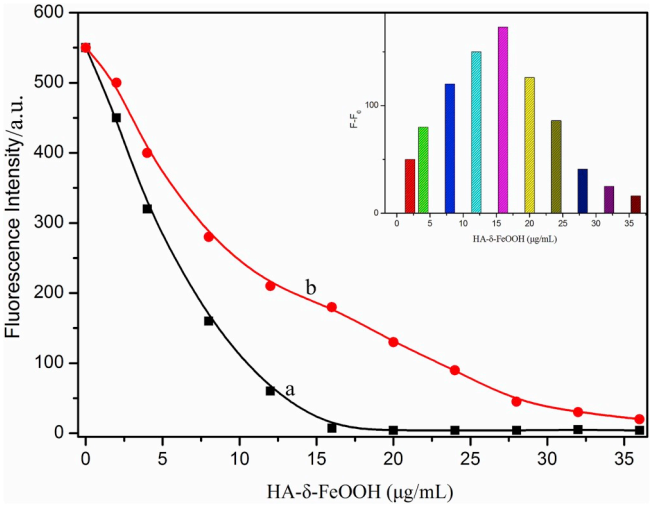

Fig. 3. The effect of HA-δ-FeOOH concentration on the fluorescence response of the sensing system in the absence (curve a) and presence (curve b) of HAase. The inset shows the fluorescence enhancement of sensing system by 10 ng/mL HAase as a function of HA-δ-FeOOH concentration. [Si QDs] = 0.02 mg/mL.

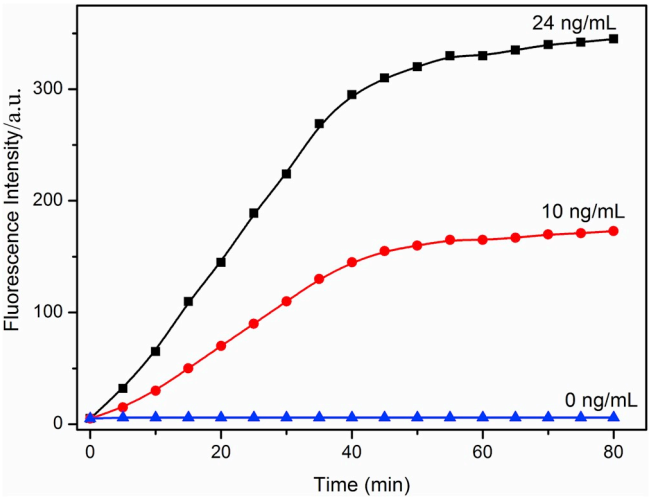

Fig. 4. Time-dependent fluorescence intensity of the sensor system with and without HAase. [Si QDs] = 0.02 mg/mL, [HA-δ-FeOOH] = 17 μg/mL.

quenched (curve b), which indicates that the δ-FeOOH could also quench the fluorescence of Si QDs. However, when adding the same amount HA-δ-FeOOH, the quenching efficacy is about 90% (curve d). It is maybe that the formation of Si QDs/HA-δ-FeOOH nanoprobes induces fluorescence quenching through an electrostatic interaction. Because of the magnetic properties of δ-FeOOH nanosheets, under the action of an external magnetic field, the background signal was greatly reduced and even to eliminate background signal (curve e). In the presence of HAase, HA is enzymatically cleaved to small fragments, the Si QDs release from the surface of δ-FeOOH and their fluorescence is correspondingly recovered (curve c). The gel electrophoresis method was used to validate experimental feasibility. As shown in Fig. S18, the pure HA had an average molecular mass of approximately 1100 kDa (lane 2). After treatment with hyaluronidase, smaller molecular mass sizes were obtained (as shown in lane 3). This indicated that HA could be digested into smaller sizes by hyaluronidase. Additionally, the HA-δ-FeOOH was treated with hyaluronidase, the similar gel electrophoresis results were obtained (lane 4 and lane 5). These results were demonstrated that δ-FeOOH nanosheets did not affect the activity of HAase for digesting HA on the surface of HA-δ-FeOOH in this experiment. These results imply that the designed method could be adopted to measure the amount of HAase.

3.3. Optimization of experimental conditions

To reach the optimal detection performance, we optimized the sensing conditions including the amount of HA-δ-FeOOH and the reaction time of HAase with Si QDs/HA-δ-FeOOH. The result proved that the concentration of HA-δ-FeOOH was one of the key elements in the detection assay. When the concentration of HA-δ-FeOOH was in a very low does, the background signal was high. It was probably because of the incomplete absorption of Si QDs on the surface of HA-δ-FeOOH. However, when HA-δ-FeOOH concentration was too high, the Si QDs released from the enzyme digestion would be adsorbed on the excessive amount of HA-δ-FeOOH nanosheets, resulting in a small recovery the fluorescence. Therefore, there was a necessity to optimize the content of HA-δ-FeOOH to obtain the highest fluorescence enhancement effect. It was implied in Fig. 3 that the enhanced fluorescence intensity ($F–F_0$, where F_0 and F were the fluorescence intensities in the absence and presence of HAase, respectively.) of the sensing assay increased greatly with increasing the concentrations of HA-δ-FeOOH from 0 to 17 μg/mL. When the concentration of HA-δ-FeOOH was more than 17 μg/mL, the

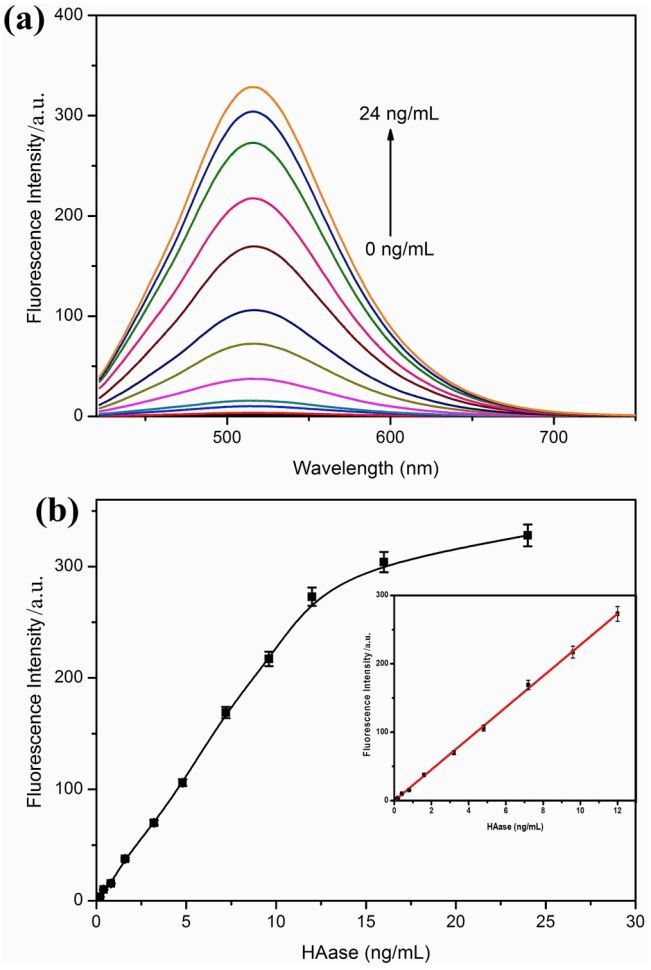

Fig. 5. (a) Fluorescence emission spectra of the Si QDs/HA-δ-FeOOH system after incubation with different concentrations of HAase: 0, 0.1, 0.2, 0.4, 0.8, 1.6, 3.2, 4.8, 7.2, 9.6, 12, 16 and 24 ng/mL; (b) the relationship between the fluorescence intensity and the concentration of HAase. The inset shows the linear relationship in the concentration ranging from 0.1 to 12 ng/mL. The error bar was calculated from three independent experiments.

enhanced fluorescence intensity ($F–F_0$) descend with a further increase of HA-δ-FeOOH concentration. Therefore, 17 μg/mL of HA-δ-FeOOH was considered as the best concentration in further experiments.

The enzyme cleavage time also affects the detection performance of nanoprobe. HA can be broken down into small molecular by HAase through enzymatic hydrolysis, and as a result, the intensity of the recovery fluorescence signal was related to the time of enzymatic hydrolysis interaction. Fig. 4 shows that the intensity of Si QDs/HA-δ-FeOOH complexes increased significantly with the increase of the enzymatic hydrolysis time and reached a plateau after 60 min, indicating that 60 min was enough for the enzymatic hydrolysis of HAase and Si QDs/HA-δ-FeOOH.

3.4. Sensitivity of Si QDs/HA-δ-FeOOH sensor for HAase detection

The fluorescence spectra of the sensing assay, which were incubated with various concentrations of HAase were investigated when it was under the most appropriate conditions. It was shown in Fig. 5a that, the obvious fluorescence intensity increased when increasing concentrations of HAase. Owing to the significant fluorescence increasing, noticeable fluorescence color changes from colorless to green could be observed under a UV lamp (Fig. S19). By measuring the fluorescence intensity of the nanoprobe upon addition of a various amount of HAase, the working curve for HAase concentration ranging from 0.1 to 24 ng/mL was obtained (Fig. 5b). The inset in Fig. 5b showed a linear response to the concentration of HAase over the range of 0.1 to 12 ng/mL. The correlation equation was $F = 22.793 \times [HAase]\ (ng/mL) + 4.396$ ($R=0.997$). The detection limit was 0.02 ng/mL (equal to 0.0127 mU/mL) based on $3\sigma/S$ (where σ is the standard deviation of blank measurements and is measured as 0.152 ($n = 11$), the S is the slope of the linear equation) (Sun et al., 2011; Wang et al., 2014). In comparison with other sensor platforms for HAase detection (Table S1), this platform detection limit is three orders of magnitude lower than that of most of the previous reported fluorescence sensors for HAase. The reasons may be that in most sensor system, the chromophores dissociate from the quencher after enzyme digestion, and the fluorescence of chromophores was recovered. However, the quencher was still keeping in the solution, which still impacts the emitted light of dissociating chromophores and influence trace detection. In our sensor system, after enzyme digestion, the quencher was separated from the solution by using a magnetic field, which would not impacts the emitted light of dissociating Si QDs, thus the detection sensitivity was enhanced (as shown in Fig. S20).

3.5. Selectivity of Si QDs/HA-δ-FeOOH sensor for HAase detection

In order to measure specificity of the prepared nano-biosensor for the detection of HAase, we exposed the system to a series of potential interferences such as heparinase I, chondroitinase ABC (ChSase ABC), lactase, pectinase, human serum albumin (HSA), glucose (Glu), glutathione (GSH), alkaline phosphatase (ALP), cysteine (Cys), thrombin, lysozyme, trypsin, NaCl and KCl under the same experimental environment as those for HAase. As shown in Fig. 6 that only HAase can lead to the fluorescence recovery of the Si QDs/HA-δ-FeOOH nanoprobe. It was also shown that the un-specific reacting enzymes could not digest HA, and thus it could not release Si QDs from the surface of HA-δ-FeOOH to induce fluorescence recovered. Additionally, it can be seen that other proteins or small molecules had no vital and effective impact on the detection of HAase, which shows that there exists an important specificity toward HAase in the proposed strategy. These findings illustrated valuable assay selectivity for HAase.

3.6. HAase detection in urine samples

Because of the importance of HAase detection in clinical diagnosis, the urine samples from three advanced bladder cancer men patients, three early bladder cancer men patients, and three healthy men peoples were prepared to estimate the applicability of our method. The level of HAase in the nine urine samples was evaluated through the commercial ELISA kit (Kamiya Biomedical Company, California, USA) and our designed method, respectively. It should be noted that the detection of HAase activity by using ELISA method was independently performed in the Henan Cancer Hospital. From the detection results in Table 1, we can find that the results obtained for our designed method are in accordance with that obtained using the commercial ELISA kit approach. It indicates that our sensing system could be used to biological samples. What is more, it could be observed that when the grade of bladder cancer increased, the level of HAase greatly increased. The HAase concentrations in urine specimens from advanced bladder cancer patients increased several times higher than that of the group of normal healthy people, which shows a similar tend with the previous reports (Lokeshwar et al., 1998; Pham et al., 1997).

Table 1
Comparisons of this method with the traditional ELISA kit method, for the detection of HAase in the urine samples.

Sample [a]	This work (ng/mL)[b]	RSD (%, n=3)	ELISA (ng/mL)[b]	RSD (%, n=3)
1	168.8	2.5	165.4	2.6
2	195.2	2.3	192.8	2.4
3	178.4	2.2	179.2	2.1
4	95.5	2.6	96.2	2.9
5	78.5	2.4	79.2	2.4
6	82.7	1.9	80.9	2.7
7	17.5	3.2	18.0	3.0
8	18.6	2.8	18.9	3.1
9	17.7	3.1	17.0	2.9

[a] Samples 1, 2 and 3 were from advanced bladder cancer patients; samples 4, 5 and 6 were from early bladder cancer patients; 7, 8, 9 were from healthy peoples.
[b] Each sample was analyzed in triplicate, and the results were the average values.

4. Conclusions

In conclusion, we have developed a background-eliminated fluorescence assay based on δ-FeOOH nanosheet and green fluorescence Si QDs for highly efficient detection of HAase. This approach has lots of advantages including high sensitivity, excellent specificity and simplicity. By using fluorescence quenching and magnetic separation ability of δ-FeOOH, this strategy exhibit a detection limit of 0.0127 mU/mL for HAase. This is much 1000 times lower than the fluorescence biosensors which were reported previously. In addition, the proposed approach has the ability to detect the target in complex biological samples including urine samples. For this reason, we expect that this strategy would be widely applied in various areas, such as medical diagnostics and biological.

Declaration of competing interest

The authors declare that they have no known competing financial interests or personal relationships that could have appeared to influence the work reported in this paper.

CRediT authorship contribution statement

Xiang Li: Conceptualization, Data curation, Investigation, Visualization, Writing - review & editing. **Tian Wu:** Conceptualization, Data curation, Investigation, Formal analysis, Writing - original draft. **Yuanqi Fu:** Formal analysis. **Xuelian Ding:** Methodology, Formal analysis. **Zhongjian Li:** Methodology, Resources. **Guifen Zhu:** Formal analysis, Resources. **Jing Fan:** Supervision, Validation, Funding acquisition, Project administration, Writing - review & editing.

Acknowledgements

This work was supported by the National Natural Science Foundation of China (Grant No. 21705034 and 21777038), the Key scientific research project of higher education of the Henan province (18A150032), Dr. start-up project funding of Henan Normal University (qd16116) and program for innovative research team in science and technology in university of Henan province (No.20IRTSTHN011)

Appendix A. Supplementary data

Supplementary data to this article can be found online at https://doi.org/10.1016/j.bios.2019.111928.

References

Anichini, C., Czepa, W., Pakulski, D., Aliprandi, A., Ciesielski, A., Samorì, P., 2018. Chem. Soc. Rev. 47, 4860–4908.
Baptista, F.R., Belhout, S.A., Giordani, S., Quinn, S.J., 2015. Chem. Soc. Rev. 44, 4433–4453.
Brannon, J.H., Magde, D., 1978. J. Phys. Chem. 82, 705–709.
Chen, P.Z., Xu, K., Li, X.L., Guo, Y.Q., Zhou, D., Zhao, J.Y., Wu, X.J., Wu, C.Z., Xie, Y., 2014. Chem. Sci. 5, 2251–2255.
Chinen, A.B., Guan, C.M., Ferrer, J.R., Barnaby, S.N., Merkel, T.J., Mirkin, C.A., 2015. Chem. Rev. 115, 10530–10574.
Faria, M.C.S., Rosemberg, R.S., Bomfeti, C.A., Fernando, M.D.S., Oliveira, L.C.A., Rodriguez, M., Pereira, M.C., Rodrigues, J.L., 2014. Chem. Eng. J. 237, 47–54.
Fan, H., Huang, X., Shang, L., Cao, Y.T., Zhao, Y.F., Wu, L.Z., Tung, C.H., Yin, Y.D., Zhang, T.R., 2016. Angew. Chem. Int. Ed. 55, 2167–2170.
Ge, J., Cai, R., Yang, L., Zhang, L.L., Jiang, Y., Yang, Y., Cui, C., Wan, S., Chu, X., Tan, W. H., 2018. ACS Sustain. Chem. Eng. 6, 16555–16562.
Gu, W., Yan, Y.H., Zhang, C.L., Ding, C.P., Xian, Y.Z., 2016. ACS Appl. Mater. Interfaces 8, 11272–11279.
Hu, S.S., Ouyang, W.J., Guo, L.H., Lina, Z.Y., Jiang, X.H., Qiu, B., Chen, G.N., 2017. Biosens. Bioelectron. 92, 718–723.
Li, X.Q., Zhou, Z., Zhang, C.C., Zheng, Y.H., Gao, J.W., Wang, Q.M., 2018. Inorg. Chem. 57, 8866–8873.
Lin, G., Gao, C.H., Zheng, Q., Lei, Z.X., Geng, H.J., Lin, Z., Yang, H.H., Cai, Z.W., 2017. Chem. Commun. 53, 3649–3652.
Liu, B., Wang, Y., Peng, H.Q., Yang, R.O., Jiang, Z., Zhou, X.T., Lee, C.S., Zhao, H.J., Zhang, W.J., 2018. Adv. Mater. 30, 1803144–1803152.
Liu, J.W., Wang, Y.M., Zhang, C.H., Duan, L.Y., Li, Z., Yu, R.Q., Jiang, J.H., 2018. Anal. Chem. 90, 4649–4656.
Liu, Q.L., Xu, S.H., Niu, C.X., Li, M.F., He, D.C., Lu, L., Ma, L., Na, N., Huang, F., Jiang, H., Ouyang, J., 2015. Biosens. Bioelectron. 64, 119–125.
Liu, S.Y., Zhao, N., Cheng, Z., Liu, H.G., 2015. Nanoscale 7, 6836–6842.
Lima, L.V.C., Rodriguez, M., Freitas, V.A.A., Souza, T.E., Machado, A.E.H., Patrocínio, A. O.T., Fabris, J.D., Oliveira, L.C.A., Pereira, M.C., 2015. Appl. Catal., B 165, 579–588.
Lokeshwar, V.B., Estrella, V., Lopez, L., Kramer, M., Gomez, P., Soloway, M.S., Lokeshwar, B.L., 2006. Cancer Res. 66, 11219–11227.
Lokeshwar, V.B., Soloway, M.S., Block, N.L., 1998. Cancer Lett. 131, 21–27.
Maia, L.F.O., Hott, R.C., Ladeira, P.C.C., Batista, B.L., Andrade, T.G., Santos, M.S., Faria, M.C.S., Oliveira, L.C.A., Monteiro, D.S., Pereira, M.C., Rodrigues, J.L., 2019. Chemosphere 215, 422–431.
Niu, W.F., Fan, L., Nan, M., Li, Z.B., Lu, D.T., Wong, M.S., Shuang, S.M., Dong, C., 2015. Anal. Chem. 87, 2788–2793.
Okamoto, S., 1968. J. Am. Ceram. Soc. 51, 594–598.
Pham, H.T., Block, N.L., Lokeshwar, V.B., 1997. Cancer Res. 54, 778–873.
Roberts, J.J., Elder, R.M., Jayaraman, A., Bryant, S.J., 2014. Biomacromolecules 15, 1132–1141.
Sinh, D.A., Lu, X.B., Wu, L.X., Tan, D.Q., Li, Y., Chen, J.P., Jain, R., 2018. Trends Anal. Chem. 98, 174–189.
Song, B., Zhong, Y.L., Wu, S.C., Chu, B.B., Su, Y.Y., He, Y., 2016. J. Am. Chem. Soc. 138, 4824–4831.
Sun, C.D., Shi, W., Song, Y.C., Chen, W., Ma, H.M., 2011. Chem. Commun. 47, 8638–8640.
Wang, C.Q., Qian, J., An, K.Q., Huang, X.Y., Zhao, L.F., Liu, Q., Hao, N., Wang, K., 2017. Biosens. Bioelectron. 89, 802–809.
Wang, Y.Q., Yan, B., Chen, L.X., 2013. Chem. Rev. 113, 1391–1428.
Wang, J., Ye, D.X., Liang, G.H., Chang, J., Kong, J.L., Chen, J.Y., 2014. J. Mater. Chem. B 2, 4338–4345.
Wang, W., Li, Y.M., Cheng, L., Cao, Z.Q., Liu, W.G., 2014. J. Mater. Chem. B 2, 46–48.
Wang, Z., Li, X.H., Feng, D., Li, L.H., Shi, W., Ma, H.M., 2014. Anal. Chem. 86, 7719–7725.
Wu, L., Qu, X.G., 2015. Chem. Soc. Rev. 44, 2963–2997.
Xu, J.J., Zhao, W.W., Song, S.P., Fan, C.H., Chen, H.Y., 2014. Chem. Soc. Rev. 43, 1601–1611.
Yang, P., Xu, Q.Z., Jin, S.Y., Zhao, Y., Lu, Y., Xu, X.W., Yu, S.H., 2012. Chem. Eur J. 18, 1154–1160.
Yin, B.F., Wang, Y., Dong, M.L., Wu, J., Ran, B., Xie, M.X., Joo, S.W., Chen, Y.P., 2016. Biosens. Bioelectron. 86, 996–1002.
Zhang, H.Y., Lin, L., Zeng, X.X., Ruan, Y.J., Wu, Y.N., Lin, M.G., He, Y., Fu, F.F., 2016. Biosens. Bioelectron. 78, 73–79.
Zhu, C.Z., Du, D., Lin, Y.H., 2017. Biosens. Bioelectron. 89, 43–55.